J Nanostruct 13(4): 999-1011, Autumn 2023

RESEARCH PAPER

The Effect of the Number of Pulses on Hybrid Nanostructures of Si NWs/Graphene / ZnO NPs Using Pulsed Laser Deposition (PLD)

Sumaya J. Abbas Alshareefi, Amer Al-Nafiey *

Collage of Sciences for Women, University of Babylon, Hillah, Iraq

ARTICLE INFO

Article History:
Received 12 June 2023
Accepted 23 September 2023
Published 01 October 2023

Keywords:
Electronic Photodetecor
Graphene
Graphene oxide
Si NWs
Zinc oxide

ABSTRACT

This paper succeeded in fabricating and characterizing hybrid nanostructures of Si NWs/graphene and ZnO NPs using pulsed laser deposition (PLD)and by different numbers of pulses (200p, 300p, 400p, 500p). where Characterization of the crystallographic, morphological, and optical properties such as XRD, FE-SEM , AFM and Diffuse reflectance for the synthesized hybrid nanosystems revealed that the addition of graphene and ZnO nanoparticles led to increased roughness values and changes in the surface topography of the membranes.

How to cite this article
Alshareefi S., Al-Nafiey A. The Effect of the Number of Pulses on Hybrid Nanostructures of Si NWs/Graphene / ZnO NPs Using Pulsed Laser Deposition (PLD). J Nanostruct, 2023; 13(4):999-1011. DOI: 10.22052/JNS.2023.04.009

INTRODUCTION

In recent years, there has been a growing demand for efficient and sustainable devices. This has led to an increased interest in novel materials with enhanced optoelectronic properties. Silicon nanowires (Si NWs) and graphene are two promising candidates for these applications due to their exceptional electrical, mechanical, and optical properties [1,2].

Si NWs have a unique one-dimensional morphology that allows for superior charge carrier mobility and efficient light absorption. Graphene, a two-dimensional carbon allotrope, exhibits exceptional electrical conductivity and high mechanical strength. By integrating these two materials, the resulting Si NWs/graphene composite can harness their individual advantages, leading to improved device performance and functionality[3].

The incorporation of functional nanomaterials, such as zinc oxide nanoparticles (ZnO NPs), can further enhance the performance of these hybrid nanostructures. ZnO NPs possess excellent optical properties, such as a wide bandgap and high exciton binding energy, making them suitable for applications in optoelectronic devices. Moreover, their unique surface chemistry allows for easy functionalization, enabling tailored interactions with the Si NWs and graphene matrix [4,5].

Graphene and ZnO NPs have also been combined with silicon nanowire substrates to create high-performance detectors. These detectors have shown promise for applications in a variety of fields, including security, environmental monitoring, and medical diagnostics [6].

The combination of Si NWs, graphene, and

* *Corresponding Author Email: amer76z@yahoo.com*

ZnO NPs offers a promising platform for the development of next-generation optoelectronic devices. These hybrid nanostructures have the potential to revolutionize a wide range of applications, from energy harvesting to medical diagnostics[7].

Graphene and reduced graphene oxide (rGO) have been extensively studied for their photoresponse properties. The 3D interconnected bicontinuous rGO network demonstrates superior photon-to-photocurrent conversion, attributed to enhanced light absorption, photocarrier transport, and tunable oxygenation and reduction states.

The combination of Si NWs, graphene, and ZnO NPs offers the potential for synergistic effects and enhanced material properties. Researchers have proposed several approaches to integrate these materials, such as incorporating ZnO NPs onto Si NWs or graphene surfaces, growing Si NWs or ZnO NPs directly on graphene sheets, and creating composite structures by mixing Si NWs, graphene, and ZnO NPs. These hybrid structures can exploit the unique properties of each constituent material. [8].

The manufacturing and integration of Si NWs, graphene, and ZnO NPs offer exciting prospects for various applications. Researchers have explored different synthesis methods to create hybrid structures that harness the unique properties of each material. The combination of Si NWs, graphene, and ZnO NPs shows promise in electrical and optoelectronic devices, energy storage and conversion systems, as well as environmental and biomedical applications. Further research and development are necessary to fully explore the potential of these materials and unlock their synergistic effects.[9].[10].

Through previous research, it is evident that the combination of graphene or ZnO NPs on a substrate of silicon nanowires has been achieved using various methods, including laser ablation. Among these methods, pulsed laser deposition (PLD) stands out as a popular technique for nanoparticle fabrication. PLD involves the use of a laser to vaporize a target material within a vacuum chamber, resulting in its condensation onto a substrate to form a thin film or coating [11]. This technique offers precise control over the thickness and composition of the deposited material, enabling the production of well-defined and high-quality coatings. PLD is widely employed in the synthesis of thin films for electronic and optical applications, as well as in the creation of nanostructured materials [12]. One notable advantage of PLD is its ability to produce films with consistent thickness and composition, which proves beneficial for various applications [13].

This study will focus on the synthesis and fabrication of hybrid nanostructure systems of Si NWs/graphene and ZnO NPs by PLD, the effect of the number of laser pulses on the fabrication process, and the characterization of the optical and electrical properties of the composite hybrid nanostructure systems.

MATERIALS AND METHODS

In the research, high-purity materials were used to ensure reliable and accurate results. The silicon wafer used was a p-type model with a crystal orientation of 110, and a purity of 99.99%. The wafer was purchased from a reputable company Henan CXH Purity-China, with a standard-GB specification. Nitric acid was used in the research, and its concentration was 65.9%. The acid was obtained from Sigma Aldrich-China, a trusted supplier of laboratory chemicals and materials. Graphite powder with a purity of 99.99% was also purchased from Sigma Aldrich-China. Hydrofluoric acid (99.9% purity) was used in the study and obtained from a reliable company Henan CXH Purity-China. Silver nitrate powder (99.99% purity) and zinc metal powder (99.99% quality) were used, and the zinc was n-type with a model purchased from Shenzhen Rearth Technology Co. Limited, a reputable supplier based in China.

Silicon nanowires (SiNWs) were chemically synthesized to have a large interaction area. A 2 x 2 cm piece of silicon was cleaned well with ethanol alcohol and distilled water to remove fingerprints and dust. The silicon piece was then placed in a solution of silver nitrate (AgNO3) 0.03 grams, hydrofluoric acid (HF) 5M, and distilled water (deionized twice) for 3 hours. This solution protected the silicon piece from acidic corrosion and allowed for a moderate and homogeneous chemical etching. After 3 hours, the silicon sample was lifted by plastic forceps from the ends of the complex solution and placed in nitric acid (HNO_3) to remove the silver nitrate and acid residue (HF). The sample was then lifted and placed in distilled water again to remove any plankton. Finally, the sample was taken outside and left to dry [24].

Graphite and zinc oxide were compressed into discs. The graphite disc was prepared by

crushing and grinding graphite in an amount of approximately 10 grams for half an hour. The graphite powder was then kneaded with ethanol alcohol and pressed in a hydraulic press under pressure not exceeding approximately 7 tons. The zinc oxide disc was prepared in a similar manner.

SiNWs, graphene, and ZnO nanoparticles were then deposited on the silicon nanowires by pulsed laser deposition (PLD). The PLD process was carried out in a vacuum chamber under vacuum pressure of 10^{-4} m bar. The graphene nanoparticles were prepared by shining a Q-Switching Nd: YAG pulsed laser beam at an angle of 45° on the graphite disc fixed on a rotating substrate. The wavelength of the laser beam was 1064 nm, the energy was 700 mJ, the frequency was 6 Hz, and the number of pulses was 500. A substrate (Si NW) was placed a few distances from the disc and heated to facilitate particle cohesion. The zinc oxide nanoparticles were prepared in a similar manner, as in Fig. 1.

The samples are labeled as follows:

Si NWS- G -ZnO NPs …(200p): Thin films of graphene, and zinc oxide nanoparticles on the. silicon nanowires,S1

Si NWS- G -ZnO NPs …(300p): Thin films of graphene, and zinc oxide nanoparticles on the. silicon nanowires,.S2

Si NWS- G -ZnO NPs …(400p): Thin films of graphene, and zinc oxide nanoparticles on the. silicon nanowires,S3

Si NWS- G -ZnO NPs …(500p): Thin films of graphene, and zinc oxide nanoparticles on the. silicon nanowires, S4

The nanocomposite device was fabricated by depositing thin layers of graphene and zinc oxide nanoparticles on a silicon oxide nanowire substrate by PLD. Then silver electrodes were placed on the device, one of which was directly on the silicon oxide nanowire and the other on the thin layer of zinc oxide nanoparticles. The electrodes were connected to a potentiometer, as shown in Fig. 2.

RESULTS AND DISCUSSION

The hybrid nanostructures of Si NWs/graphene and ZnO NPs were fabricated and characterized

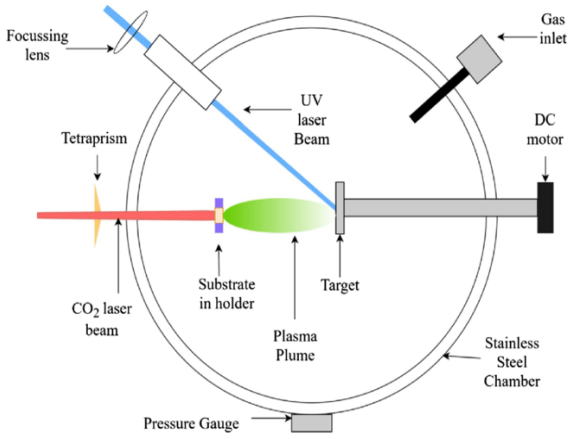

Fig. 1. Vacum chamber PLD .

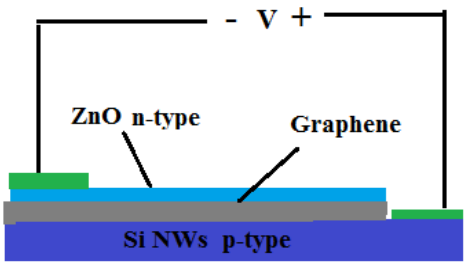

Fig. 2. Preparation of the nanocomposite system (Si NWs/G, ZnO NPS)

using pulsed laser deposition (PLD) and with different numbers of pulses (200p, 300p, 400p, 500p). and analyzed using different characterization techniques such as thickness measurement (Ellipsometer), X-ray diffraction (XRD), atomic force microscopy (AFM), and scanning electron microscopy (SEM). Interpretation of these results provides valuable insights into the structural and morphological properties of the investigated materials.

Structural and Morphological Properties
Thickness Measurement (Ellipsometer)

To determine the thickness of the deposited films, an Ellipsometer interferometer from Holark was employed. This technique relies on the interference of a light beam reflected from the surface of the thin film and the bottom of the substrate. A He-Ne laser with a wavelength of 600 nm was utilized in the measurements. The obtained thickness values of the thin films are

Table 1. Samples Parameters and Film thickness for all the prepared films.

Samples	Material	Pulses	Film Thickness (nm)
S1	SiO NWS/G, ZnO NPs	200	150
S2	SiO NWS/G, ZnO NPs	300	155
S3	SiO NWS/G, ZnO NPs	400	161
S4	SiO NWS/G, ZnO NPs	500	173

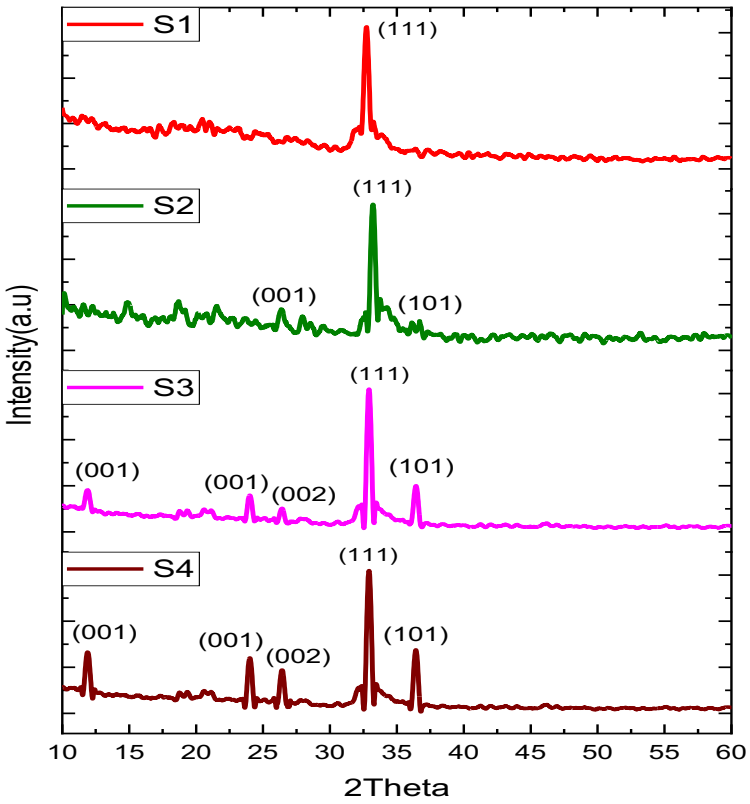

Fig. 3. X-ray diffraction (S1,S2,S3 and S4)

summarized in Table 1.

The table shows the thickness of thin films prepared by pulsed laser deposition (PLD). The thickness of the thin films increases with the number of pulses used to deposit them. This is because the number of pulses determines the amount of material deposited on the substrate. The thickness of the thin films also increases with the addition of graphene and zinc oxide nanoparticles. This is because graphene and zinc oxide nanoparticles are larger than silicon oxide nanowires, so they take up more space on the substrate.

X-ray diffraction tests (XRD)

The X-ray diffraction (XRD) patterns of the Si NWs, Si NWs/GO, Si NWs/ZnO, and Si NWs/G/ZnO thin films are shown in Fig. 3. The XRD patterns show that all of the thin films are polycrystalline with a cubic phase. The sharp peaks in the

Table 2. values of crystalline levels and mid-width at the highest intensity and crystal sizes for samples.

Films	(hkl)	2 θ (deg)	FWHM	C.S(nm)	Avg C.S
Si NWs/G, ZnO NPs (200P)	SiONW(111)	32.74	0.28	26.22	25.85
	ZnO(101)	36.48	0.29	25.45	
	G (002)	26.91	0.29	25.88	
Si NWs/G, ZnO NPs (300P)	Si (211)	33.22	0.28	26.27	26.61
	ZnO(101)	36.37	0.29	26.62	
	G (002)	26.13	0. 28	27.03	
Si NWs/G, ZnO NPs (400P)	SiONW(111)	32.93	0.25	29.04	28.51
	ZnO(101)	36.18	0.28	26.07	
	G (002)	26.16	0.25	29.72	
	GO (001)	11.16	0.26	29.22	
Si NWs/G, ZnO NPs (500P)	SiONW(111)	32.93	0.15	47.17	40.99
	ZnO (101)	36.41	0.16	46.14	
	G (002)	26.37	0.17	44.02	
	rGO (001)	24.00			
	GO (001)	11.91	0.17	26.64	

Table 3. AFM parameters for Samples thin films. (Ra) Roughness and (RMS) Root Mean Square.

Samples	Ra(nm)	RMS(nm)	Ave. Particle Size (nm)
Si NWS/G, ZnO NPs (200P)	2.28	3.12	15.73
Si NWS/G, ZnO NPs (300P)	2.77	3.62	17.86
Si NWS/G, ZnO NPs (400P)	3.55	4.45	20.89
Si NWS/G, ZnO NPs (500P)	6.20	7.95	40.45

XRD patterns correspond to the characteristic diffraction peaks of Si, GO, ZnO, and Si.

The XRD pattern of the Si NWs thin film shows peaks at 32.92°, 33.14°, 28.45°, and 47.98°, which correspond to the (111), (201), (111) and Si (220) planes of Si , respectively according to standard [00-027-1402] , this result is consistent with the studies [17- 19]. The XRD pattern of the Si NWs/GO thin film shows peaks at 32.92°, 26.36°, and 11.45°, which correspond to the (111) plane of Si , the (002),(001) plane of G,GO, and a broad peak related to the interlayer distance between graphene oxide sheets, respectively , this result is consistent with the studies [20,21]. The XRD pattern of the Si NWs/ZnO thin film shows peaks at 32.92°, 33.91°, 36.24°, and 56.15°, which correspond to the (111), (301), (101), and (110) planes of ZnO, respectively [22,23]. The XRD pattern of the Si NWs/G/ZnO thin film shows peaks at 32.92°, 36.41°, 26.37°, 24.00°, and 11.91°, which correspond to the (111) plane of Si , the (101) plane of ZnO, the (001),(002) plane of rGO, GO, and a broad peak related to the interlayer distance between graphene oxide sheets, respectively ,this result is consistent with the studies [17,20,22,23].

The XRD results show that the addition of GO and ZnO to the Si NWs does not significantly affect the crystalline structure of the thin films. However, there is a slight displacement in the locations of some characteristic peaks, which is likely due to the formation of chemical compounds between Si , GO, and ZnO.

The XRD-confirmed data pattern has been listed in Table 2, which showed excellent consistency

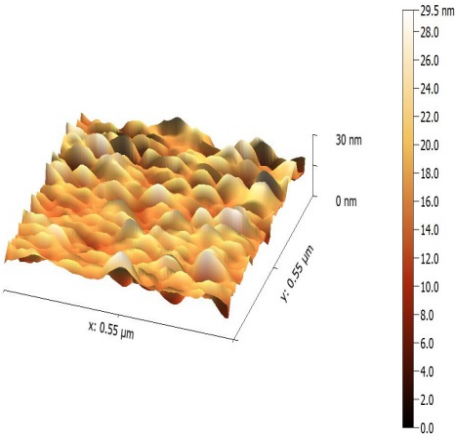

AFM images of (S1).

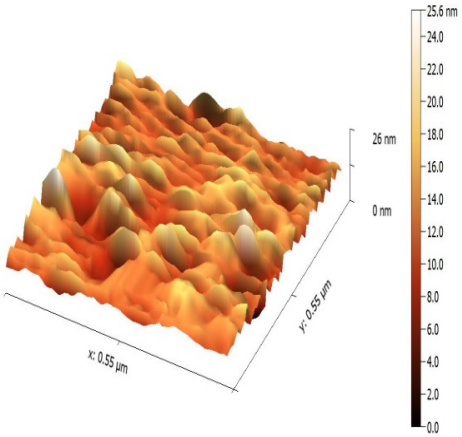

AFM images of (S2).

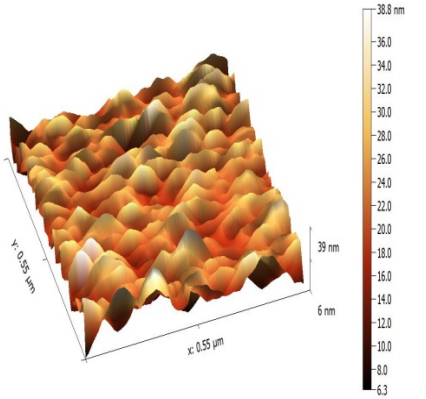

AFM images of (S3).

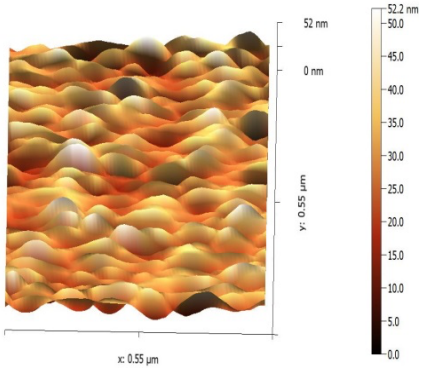

AFM images of (S4).

Fig. 4. Atomic force microscopy images of (S1, S2, S3 and S4) .

with the interplanar distance standard values.

The table shows that the XRD results for the three thin films (Si NWs, Si NWs/GO, and Si NWs/G/ZnO) show that the addition of GO and ZnO to the Si NWs causes the thin films to become more disordered. The Si NWs/G/ZnO thin film is the most disordered of the three thin films, with an average interplanar spacing of 40.99 nm, a significantly larger FWHM of the diffraction peaks, and slightly different diffraction angles than the other two thin films.

The increased disorder in the Si NWs/G/ZnO thin film is likely due to the following factors:

- The different properties of GO and ZnO. These two materials have different chemical and physical properties, which can affect the way they pack into a crystal lattice.

- The different sizes of the GO and ZnO nanoparticles. GO nanoparticles are significantly larger than ZnO nanoparticles. This means that they are more difficult to pack into a regular crystal lattice, which can lead to disorder [24] .

- The introduction of defects into the crystal structure. The addition of GO and ZnO to the Si NWs can introduce defects into the crystal structure of the thin film. These defects can be caused by the different chemical properties of GO and ZnO, as well as the different sizes of the GO and ZnO nanoparticles [25].

The crystal structure of Si NWs is hexagonal,

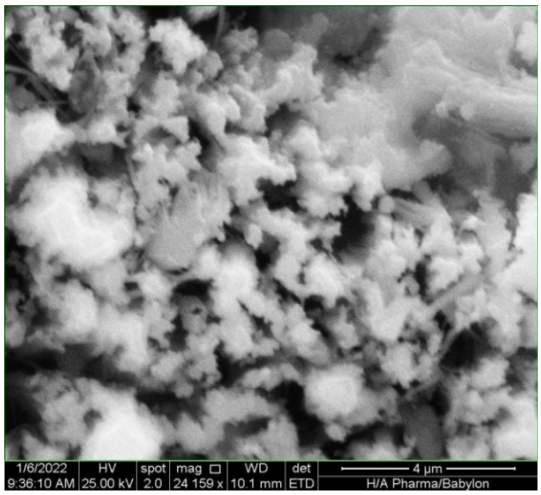

SEM images for (S1) at 200Pulse

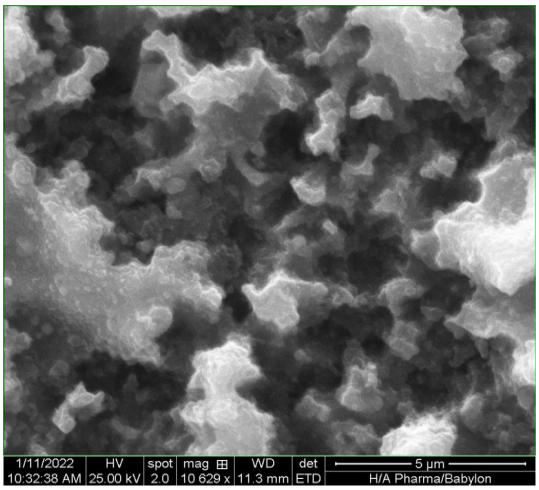

SEM images for (S2) at 300Pulse

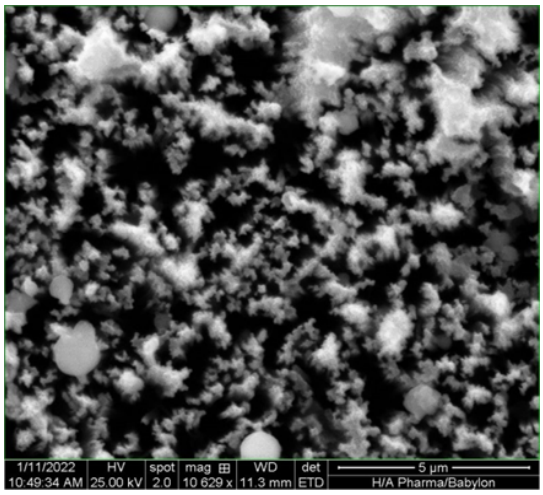

SEM images for (S3) at 400Puls

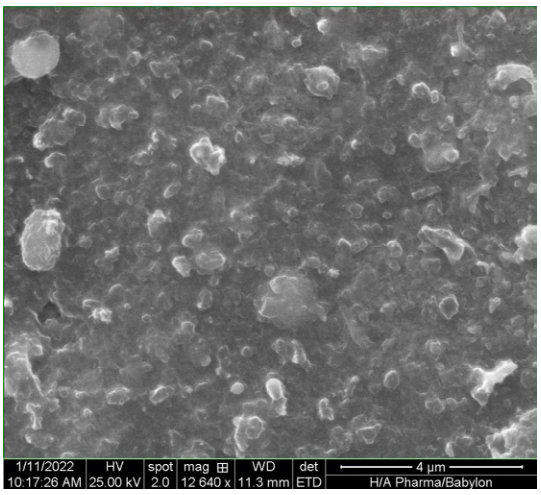

SEM images for (S4) at 500Pulse

Fig. 5. SEM images for thin films

and the addition of GO does not change the crystal structure. The reason for this is that GO, which is a two-dimensional material with a hexagonal lattice structure[26]. When GO is added to Si NWs, the GO sheets wrap around the Si NWs, maintaining the hexagonal crystal structure. but ZnO, which is a three-dimensional material with a cubic lattice structure[26]. However, when GO and ZnO are added together, the GO sheets can interact with the ZnO nanoparticles, causing the ZnO nanoparticles to rearrange themselves into a hexagonal lattice structure in the Si NWs/G/ZnO thin film.

The hexagonal crystal structure is more conductive than the cubic crystal structure, so the Si NWs/G/ZnO thin film may have better electrical properties than the Si NWs/ZnO thin film. Additionally, the hexagonal crystal structure has different optical properties than the cubic crystal structure[27], so the Si NWs/G/ZnO thin film may have different optical properties than the Si NWs/ ZnO thin film.

The increased disorder in the Si NWs/G/ZnO thin film may have introduced new energy levels into the band gap of the thin film, which could lead to new optical properties[28].

Atomic force microscopy (AFM) Tests

The surfaces of Si NWs/G/ZnO thin films prepared using the pulsed laser deposition (PLD) technique were examined using atomic force microscopy (AFM) to analyze their topography and determine important parameters such as average particle size, distribution, root mean square (RMS), and roughness (Ra). The results, as presented in Table 3, indicate a clear change in the surface topography of the samples, which is attributed to the addition of graphene (G) and zinc oxide (ZnO) nanoparticles in thin thickness on Si NWs substrate [29,30].

The highest value for the root mean square (RMS) roughness and average particle size were recorded at 6.20 nm and 40.45 nm, respectively, for the Si NWs/G/ ZnO 500 Pulse sample. The lowest values were obtained for the Si NWs sample, with RMS roughness and average particle size of 1.44 nm and 15.39 nm, respectively.

The difference in the grain size values measured by AFM and X-ray diffraction (XRD) is due to the fact that AFM measures the grain size directly, while XRD measures the crystal size using Scherrer's formula.

In Fig. 4,the 3D AFM images of the as-deposited films show the formation of agglomerated grains stacked on top of each other. This is due to the close grains clustering together to cover the uneven peaks and hills from the silicon nanowires. Increasing the G and ZnO ratios improve the crystalline structure of the Si NWs/G-ZnO films, which is in agreement with the XRD results. This leads to improving the responsivity properties of the films.

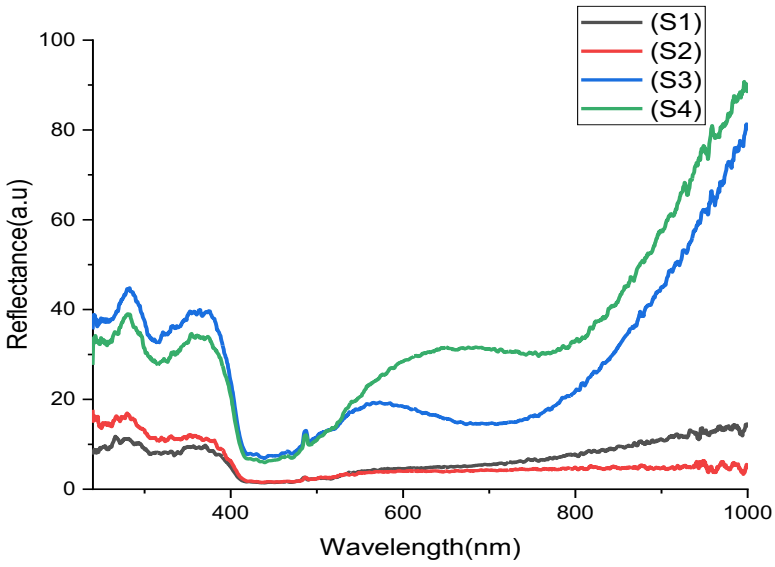

Fig. 6. The reflectivity as a function of the wavelength for all the prepared devices .

Scanning Electron Microscopy (SEM)

The SEM images presented in Fig. 5 offer valuable insights into the shape and arrangement of the silicon nanowires. It is evident from the images that the nanowires possess varying lengths and diameters, with examples of nanowires measuring 80.11 nm and 121.8 nm in diameter. The nanowires exhibit a well-organized pattern, aligning with each other on the surface.

The deposition of the graphene and ZnO nanoparticles was carried out under uniform conditions, maintaining consistent temperature, pressure, and number of pulses within the PLD deposition chamber.

Moreover, the SEM images demonstrate the successful deposition of a thin film comprising graphene and ZnO nanoparticles onto the Si NWs substrate. The graphene layer is clearly visible, serving as a protective cover encapsulating the silicon oxide nanowires [29]. Additionally, the layer of ZnO nanoparticles can be observed distributed on top of the graphene layer.

The SEM results align with the findings from the AFM measurements, indicating that the introduction of graphene and ZnO nanoparticles onto the Si NWs substrate resulted in significant changes in the surface topography of the films. The presence of the graphene layer appears to have smoothened the surface of the silicon oxide nanowires, while the ZnO nanoparticles contribute to the creation of a rougher surface.

The addition of graphene and ZnO nanoparticles led to increased roughness values and a reduction in average particle size. The enhancement of the crystalline structure observed in the Si NWs/G, ZnO films, characterized by higher G and ZnO ratios, correlates with improved responsivity properties, consistent with the XRD results.

Optical properties

The study of the optical properties of the films is of great importance in finding the optical constants through which it is possible to know the value of the optical energy gap from the reflectance by using the Kubelka-Munk theory.

Reflectance (R)

The reflectance of silicon oxide nanowires (Si NWs/G/ZnO NPs) depends on a variety of factors, including the diameter and length of the nanowires, the incident angle and polarization of light, and the refractive indices of the surrounding media.

(Si NWs/G/ZnO NPs ..200P) exhibit lower reflectance compared to (Si NWs/G/ZnO NPs ..500P) due to their enhanced light trapping and absorption properties. The increased surface area of the nanowires allows for multiple total internal reflections, which leads to a longer optical path and higher absorption of light. Additionally, the nanowire diameter of about 100 nm as in the SEM images can match the resonant wavelength of the incident light, resulting in even higher absorption.

However, the reflectance of (Si NWs/G/ZnO NPs ..200P) can also be affected by surface roughness, contamination, and other structural defects that can scatter or reflect light.

From the observations in Fig. 6, (Si NWs/G/ZnO NPs ..200P) exhibit reflectivity in the ultraviolet (UV) region at 28%, and in the visible light range of 600-1000 nm, it increases from 3% to 10%. When increases the number of pulses to (300P) in(Si NWs/G/ZnO NPs ..300P), the reflectance in the UV region increases by 42%, and in the visible light range, it increases significantly from 3% to 15%. In the infrared range, it increases from 15% to 30%. The same behavior is observed when increases the number of pulses to (400P) in(Si NWs/G/ZnO NPs ..400P). The UV reflectance increases to 75%, and in the visible region at 550 nm, it is 15%, and at 1000 nm, it is 30%. when increases the number of pulses to (500P) in(Si NWs/G/ZnO NPs ..500P), the UV reflectance is 60%, the visible region is 25%, and at 1000 nm, it is 100%.

The increased reflectance of (Si NWs/G/ZnO NPs) in the visible light range at (300 Pulse) can be linked to the increased nanoparticles from graphene and zinc oxide. This is because graphene is a highly conductive material, and it can help to reduce the surface roughness of the nanowires.

The increased reflectance of Si NWs in the UV and infrared ranges when ZnO is added can be linked to the higher refractive index of ZnO. This means that more light is reflected from the surface of the nanowires, resulting in a higher reflectance. The XRD results show that the increases in the number of pulses to (500P) and increases in nanoparticles of graphene and ZnO to Si NWs can cause the nanowires to become more strained. This strain can also contribute to the increased reflectance of the nanowires, as it can lead to the formation of localized surface plasmon resonances.

The reflectance results provide further

evidence of the impact of the increase in the number of pulses are increased nanoparticles of graphene and ZnO on the optical properties of Si NWs. The enhanced reflectivity in specific regions can be attributed to the improved light trapping, absorption, and modifications in surface properties brought about by the presence of graphene and zinc oxide in the Si NWs system.

Optical Energy Gap (Eg)

The band gap of composite (Si NWs/G/ZnO NPs at 200p,300p,400p,500p) is an important property that determines their optical and electronic properties. The band gap of (Si NWs/G/ZnO NPs) can vary depending on several factors, such as the diameter, length, and surface properties of the nanowires, as well as the method of preparation. Previous experimental studies have reported band gap values for Si NWs ranging from about 1.5 eV to 3.5 eV.

In this study, we investigated the effect of different materials on the energy gap of (Si NWs/G/ZnO NPs). We used the Kubelka-Munk theory, as shown in equation (6):

$$F = (1-R\infty)^2 / 2R\infty \quad (6)$$

Figs. 7 and 8 presents the energy gap diagrams

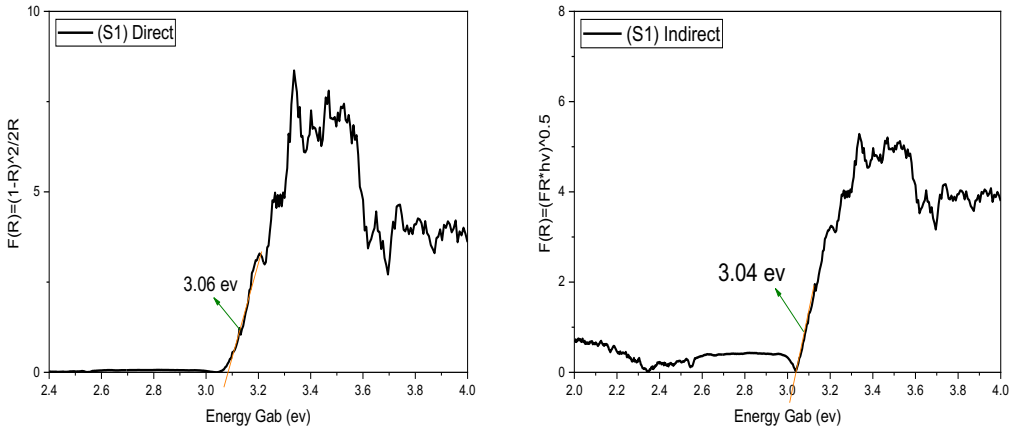

(S1) Direct **(S1) Indirect**

(S1) Si NWs/G/ZnO NPs, 200p

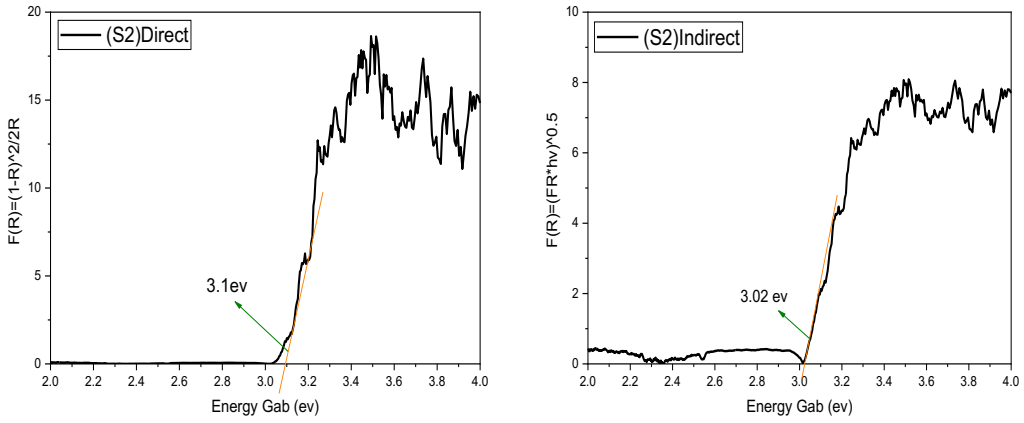

(S2) Direct **(S2) Indirect**

(S2) Si NWs/G/ZnO NPs, 300p

Fig. 7. The Energy Gap as a function of the wavelength for the S1 and S2.

for the different samples. Table 4 summarizes the direct and indirect energy gap values obtained for each sample. It was observed that the direct band gap of (Si NWs/G/ZnO NPs at 200p,300p,400p,500p) was 3.03 eV, 3.06 eV, 3.06 eV, and 3.05 eV, respectively, for the samples containing Si NWs, graphene, zinc oxide, and ternary compound. The indirect band gap of the Si NWs was 3.03 eV, 3.04 eV, 3.04 eV, and 3.04 eV, respectively, for the same samples.

Our results revealed that the energy gap of Si NWs was not significantly affected by the addition of graphene or zinc oxide, nor by the ternary compound. Specifically, the direct and indirect energy gap values of the four samples were found to be similar, indicating that the silicon nanowire base is dominant and the graphene and ZnO layers are thin nanolayers that do not significantly affect the energy gap of the Si NWs.

Our findings have important implications for the development of Si NWs-based devices, particularly in the fields of electronics, photonics, and energy conversion. By understanding the factors that influence the band gap of Si NWs, researchers can design and optimize the properties of these materials for specific applications. Furthermore,

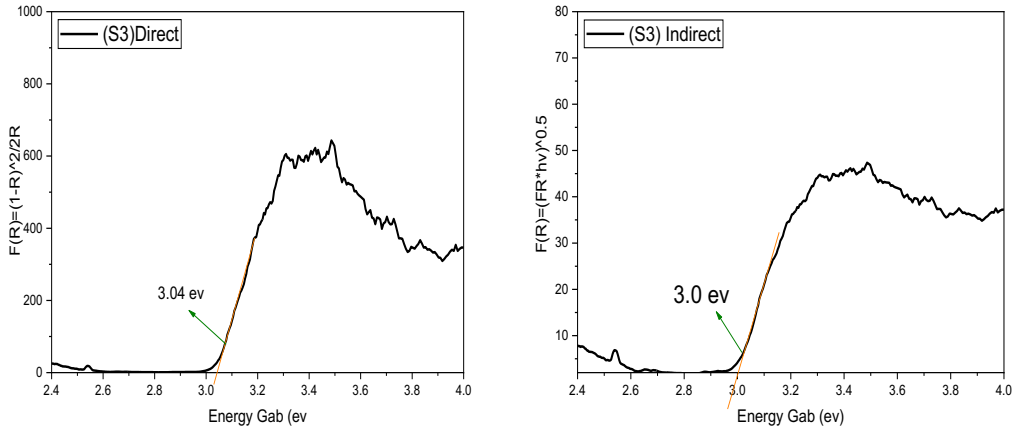

(S3) Direct **(S3) Indirect**

(S3) Si NWs/G/ZnO NPs, 400p

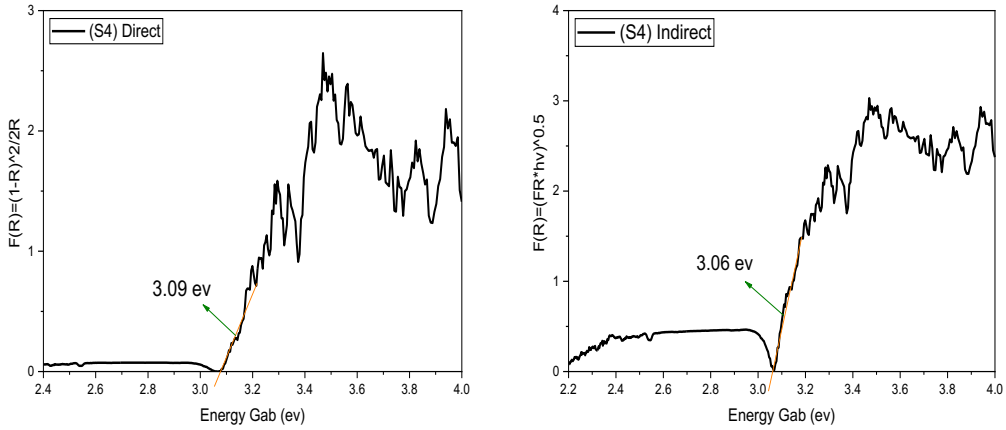

(S4) Direct **(S4) Indirect**

(S4) Si NWs/G/ZnO NPs, 500p

Fig. 8. The Energy Gap as a function of the wavelength for the S3 and S4.

Table 4. Energy Gap Values

Samples	E_g (eV) Direct	E_g (eV) Indirect
Si NWS / G, ZnO NPs (200P)	3.03	3.03
Si NWS / G, ZnO NPs (300P)	3.06	3.04
Si NWS / G, ZnO NPs (400P)	3.06	3.04
Si NWS / G, ZnO NPs (500P)	3.05	3.04

our results suggest that Si NWs combined with other materials, such as graphene and zinc oxide, may offer new opportunities for developing advanced nanomaterials with novel properties and potential applications in various fields.

CONCLUSION

This research successfully synthesized and characterized Si NWs/Graphene and ZnO NPs hybrid nanostructures using pulsed laser deposition (PLD). The crystalline, morphology, and optical properties (reflectance and energy gap) of the synthesized hybrid nanostructure systems were characterized.

The XRD results showed that the addition of GO and ZnO to the Si NWs did not significantly affect the crystalline structure of the thin films. However, there was a slight displacement in the locations of some characteristic peaks, which is likely due to the formation of chemical compounds between Si , GO, and ZnO.

The AFM results showed that The lowest values were obtained for the Si NWs sample, with RMS roughness and average particle size of 1.44 nm and 15.39 nm, respectively, and the highest value for the root mean square (RMS) roughness and average particle size were recorded at 6.20 nm and 40.45 nm, respectively, for the Si NWs/G-ZnO 500 Pulse sample.

The SEM results aligned with the findings from the AFM measurements, indicating that the introduction of graphene and ZnO nanoparticles onto the Si NWs substrate resulted in significant changes in the surface topography of the films. The presence of the graphene layer appears to have smoothened the surface of the silicon oxide nanowires, while the ZnO nanoparticles contribute to the creation of a rougher surface. The addition of graphene and ZnO nanoparticles together led to increased roughness values and a reduction in average particle size. The enhancement of the crystalline structure observed in the Si NWs/G, ZnO films, characterized by higher G and ZnO ratios, is consistent with the XRD results.

Additionally,The optical properties (reflectance and energy gap) showed that Si NWs exhibit lower reflectance than bulk silicon due to their enhanced light trapping and absorption properties. The addition of graphene and zinc oxide to Si NWs enhances the reflectivity in specific regions, including the UV and visible ranges, due to improved light trapping, absorption, and modifications in surface properties.

The energy gap of Si NWs was not significantly influenced by the addition of graphene or zinc oxide, nor by the ternary compound. Specifically, the direct and indirect energy gap values for the four samples were found to be similar, indicating that the silicon nanowire base is dominant and that the graphene and zinc oxide layers are thin nanolayers that do not significantly impact the energy gap of Si NWs.

This study provides a promising platform for the development of next-generation optoelectronic devices with broad spectral detection and high quantitative efficiency. It is expected to contribute to the advancement of various fields, including security, environmental monitoring, and medical diagnostics.

CONFLICT OF INTEREST

The authors declare that there is no conflict of interests regarding the publication of this manuscript.

REFERENCES

1. Cheng T, Zhang Y, Lai WY, Huang W. Stretchable Thin-Film Electrodes for Flexible Electronics with High Deformability and Stretchability. Adv Mater. 2015;27(22):3349-3376.
2. Ahmad W, Tareen AK, Khan K, Khan M, Khan Q, Wang Z, Maqbool M. A review of the synthesis, fabrication, and recent advances in mixed dimensional heterostructures for optoelectronic devices applications. Applied Materials Today. 2023;30:101717.
3. Bansal S, Prakash K, Sharma K, Sardana N, Kumar S, Gupta N, Singh AK. A highly efficient bilayer graphene/ZnO/silicon nanowire based heterojunction photodetector with broadband spectral response. Nanotechnology. 2020;31(40):405205.
4. Kim H, Ahn J-H. Graphene for flexible and wearable device applications. Carbon. 2017;120:244-257.
5. Ding J, Yan X, Xue Q. Study on field emission and photoluminescence properties of ZnO/graphene hybrids grown on Si substrates. Materials Chemistry and Physics. 2012;133(1):405-409.
6. AlZoubi T, Qutaish H, Al-Shawwa Ea, Hamzawy S. Enhanced UV-light detection based on ZnO nanowires/graphene oxide hybrid using cost-effective low temperature hydrothermal process. Opt Mater. 2018;77:226-232.
7. Van Khai T, Van Thu L, Ha LTT, Thanh VM, Lam TD. Structural, optical and gas sensing properties of vertically well-aligned ZnO nanowires grown on graphene/Si substrate by thermal evaporation method. Mater Charact. 2018;141:296-317.
8. Dang VQ, Trung TQ, Kim D-I, Duy LT, Hwang B-U, Lee D-W, et al. Ultrahigh Responsivity in Graphene-ZnO Nanorod Hybrid UV Photodetector. Small. 2015;11(25):3054-3065.
9. Liu H, Sun Q, Xing J, Zheng Z, Zhang Z, Lü Z, Zhao K. Fast and Enhanced Broadband Photoresponse of a ZnO Nanowire Array/Reduced Graphene Oxide Film Hybrid Photodetector from the Visible to the Near-Infrared Range. ACS Applied Materials & Interfaces. 2015;7(12):6645-6651.
10. Bansal S, Jain P, Gupta N, Singh AK, Kumar N, Kumar S, Sardana N. A Highly Efficient Bilayer Graphene-HgCdTe Heterojunction Based Photodetector for Long Wavelength Infrared (LWIR). 2018 IEEE 13th Nanotechnology Materials and Devices Conference (NMDC); 2018/10: IEEE; 2018.
11. Ogugua SN, Ntwaeaborwa OM, Swart HC. Latest Development on Pulsed Laser Deposited Thin Films for Advanced Luminescence Applications. Coatings. 2020;10(11):1078.
12. D'Andrea C, Faro MJL, Bertino G, Ossi PM, Neri F, Trusso S, et al. Decoration of silicon nanowires with silver nanoparticles for ultrasensitive surface enhanced Raman scattering. Nanotechnology. 2016;27(37):375603.
13. Bleu Y, Bourquard F, Tite T, Loir A-S, Maddi C, Donnet C, Garrelie F. Review of Graphene Growth From a Solid Carbon Source by Pulsed Laser Deposition (PLD). Frontiers in chemistry. 2018;6:572-572.
14. Important Pyroelectrics: Properties and Performance Parameters. Pyroelectric Materials: Infrared Detectors, Particle Accelerators, and Energy Harvesters: Society of Photo-Optical Instrumentation Engineers.
15. Mikla VI, Mikla VV. X-Ray Photoconductors for Direct Conversion of Digital Flat-Panel X-Ray Image Detectors. Amorphous Chalcogenides: Elsevier; 2012. p. 143-154.
16. Zhang Y, Huang P, Guo J, Shi R, Huang W, Shi Z, et al. Photodetectors: Graphdiyne-Based Flexible Photodetectors with High Responsivity and Detectivity (Adv. Mater. 23/2020). Adv Mater. 2020;32(23).
17. Yang Z, Du Y, Yang Y, Jin H, Shi H, Bai L, et al. Large-scale production of highly stable silicon monoxide nanowires by radio-frequency thermal plasma as anodes for high-performance Li-ion batteries. J Power Sources. 2021;497:229906.
18. Luo W, Wang Y, Chou S, Xu Y, Li W, Kong B, et al. Critical thickness of phenolic resin-based carbon interfacial layer for improving long cycling stability of silicon nanoparticle anodes. Nano Energy. 2016;27:255-264.
19. Xiao Z, Yu C, Lin X, Chen X, Zhang C, Wei F. Uniform coating of nano-carbon layer on SiOx in aggregated fluidized bed as high-performance anode material. Carbon. 2019;149:462-470.
20. Strankowski M, Włodarczyk D, Piszczyk Ł, Strankowska J. Polyurethane Nanocomposites Containing Reduced Graphene Oxide, FTIR, Raman, and XRD Studies. Journal of Spectroscopy. 2016;2016:1-6.
21. Surekha G, Krishnaiah KV, Ravi N, Padma Suvarna R. FTIR, Raman and XRD analysis of graphene oxide films prepared by modified Hummers method. Journal of Physics: Conference Series. 2020;1495(1):012012.
22. van Heerden JL, Swanepoel R. XRD analysis of ZnO thin films prepared by spray pyrolysis. Thin Solid Films. 1997;299(1-2):72-77.
23. Srivastava V, Gusain D, Sharma YC. Synthesis, characterization and application of zinc oxide nanoparticles (n-ZnO). Ceram Int. 2013;39(8):9803-9808.
24. Sirelkhatim A, Mahmud S, Seeni A, Kaus NHM, Ann LC, Bakhori SKM, et al. Review on Zinc Oxide Nanoparticles: Antibacterial Activity and Toxicity Mechanism. Nano-micro letters. 2015;7(3):219-242.
25. Biroju RK, Tilak N, Rajender G, Dhara S, Giri PK. Catalyst free growth of ZnO nanowires on graphene and graphene oxide and its enhanced photoluminescence and photoresponse. Nanotechnology. 2015;26(14):145601.
26. Fan Z, Huang X, Chen Y, Huang W, Zhang H. Facile synthesis of gold nanomaterials with unusual crystal structures. Nat Protoc. 2017;12(11):2367-2376.
27. Chakrabort P, Xiong G, Cao L, Wang Y. Lattice thermal transport in superhard hexagonal diamond and wurtzite boron nitride: A comparative study with cubic diamond and cubic boron nitride. Carbon. 2018;139:85-93.
28. Boruah BD, Mukherjee A, Misra A. Sandwiched assembly of ZnO nanowires between graphene layers for a self-powered and fast responsive ultraviolet photodetector. Nanotechnology. 2016;27(9):095205.
29. Gaidi M, Daoudi K, Columbus S, Hajjaji A, Khakani MAE, Bessais B. Enhanced photocatalytic activities of silicon nanowires/graphene oxide nanocomposite: Effect of etching parameters. Journal of Environmental Sciences. 2021;101:123-134.
30. Cheng C-C, Zhan J-Y, Liao Y-M, Lin T-Y, Hsieh Y-P, Chen Y-F. Self-powered and broadband photodetectors based on graphene/ZnO/silicon triple junctions. Appl Phys Lett. 2016;109(5).
31. Liu Y, Song Z, Yuan S, Xu L, Xin Y, Duan M, et al. Enhanced Ultra-violet Photodetection Based on a Heterojunction Consisted of ZnO Nanowires and Single-Layer Graphene on Silicon Substrate. Electronic Materials Letters. 2019;16(1):81-88.
32. Highly Polarization-Sensitive, Broadband, Self-Powered Photodetector Based on Graphene/PdSe2/Germanium Heterojunction. American Chemical Society (ACS).